Suplemento de la Revista Mexicana de Física **4** 021136 (2023) 1–6

Dark sector of a Higgs portal with Q4 symmetric matter

A. E. Cárcamo Hernández

Universidad Técnica Federico Santa María, and Centro Científico-Tecnológico de Valparaíso, Casilla 110-V, Valparaíso, Chile.

C. Espinoza

Cátedras Conahcyt, Departamento de Física Teórica, Instituto de Física, Universidad Nacional Autónoma de México, Apartado Postal 20-364, 01000 CDMX, México.

J. C. Gómez-Izquierdo

Centro de Estudios Científicos y Tecnológicos No 16, Instituto Politécnico Nacional, Pachuca: Ciudad del Conocimiento y la Cultura, Carretera Pachuca Actopan km 1+500, San Agustín Tlaxiaca, Hidalgo, México.

M. Mondragón

Departamento de Física Teórica, Instituto de Física, Universidad Nacional Autónoma de México, Apartado Postal 20-364, 01000 CDMX, México.

Received 20 May 2023; accepted 20 April 2023

We describe the phenomenology of the scalar and dark matter sectors of a BSM theory with Q4 symmetry among the SM fermions. The model features a Higgs portal to a dark sector comprised of heavy right-handed neutrinos. We discuss relic abundance as well as direct detection constraints on the DM candidate.

Keywords: Multi-Higgs phenomenology; discrete symmetries; dark matter.

DOI: https://doi.org/10.31349/SuplRevMexFis.4.021136

1. Introduction

The Standard Model (SM) of particle physics has become a paradigm and is considered one of humanity's greatest scientific achievements. However, it still has several unanswered questions, such as the baryon asymmetry, the muon anomalous magnetic moment, the hierarchy and strong CP problems, and the existence of dark matter. One proposed solution to these problems is the addition of discrete symmetries to the SM, which can have interesting consequences.

In Beyond the Standard Model (BSM) theories, discrete symmetries can be used to predict fermion masses. These symmetries can be spontaneously broken, resulting in realistic fermion mass hierarchies and mixing patterns. In some models, light active neutrinos have tiny masses due to an inverse seesaw mechanism mediated by three right-handed Majorana neutrinos. These models successfully accommodate experimental values of SM fermion mass and mixing parameters. Constraints on these models come from the matter sector, where fermion mass spectra and mixing patterns, as well as strong experimental limits from flavor changing neutral currents, limit these theories.

Some BSM theories propose the addition of multiple scalar doublets, as well as scalar singlets or triplets. These extensions are partially motivated by top-down theoretical constructions such as supersymmetric models, which require a minimum of two scalar doublets. Recent hints of new resonances at the Large Hadron Collider (LHC), possibly from new scalar particles, have added to the interest in these models. Although the global significance of these excesses is small, the vast amount of data yet to be collected and analyzed at the LHC makes it an exciting prospect to study the possibility of an extended scalar sector and its phenomenology.

In this letter, we briefly describe that it is also possible to constrain discrete flavor symmetries by analysing the scalar sector phenomenology, where e.g. limits from experimental scalar searches complement nicely other constraints from the matter or dark matter sectors. For brevity, we shall focus on the scalar and dark matter (DM) sectors of the $Q4$ symmetric model considered in Ref. [1], where a complete and detailed analysis can be found.

2. Q4 Model

We present an analysis for a BSM model with non-abelian $Q4$ discrete symmetry. The discrete symmetry denominated by D_N is the symmetry of a regular polygon of N sides, and occurs in nature, *e.g.*, in poly-atomic molecules. The discrete non-abelian group Q_4, also known as the binary dihedral group, can be seen as the group cover of D_4, and has pseudo-real representations which is advantageous for chiral theories. In this model we propose a scalar sector with two Higgs doublets Ξ_1, Ξ_2, and one real scalar singlet φ that

mixes with the CP-even scalar. The scalar singlet is further coupled to a right-handed heavy neutrino Ψ which is the DM candidate. We proceed to briefly describe the scalar and DM sectors phenomenology for this model.

Due to the mixing of the singlet with the real parts of the neutral scalars, we have three CP-even physical scalars, one of which corresponds to an SM Higgs-like particle h, we take the other two scalars, denoted H_3 and H as heavier. For the numerical analysis of this model, we mainly focus on collider limits for the new scalars predicted by the inclusion of the extra Higgs doublet and the phenomenology from direct detection (DD) and relic abundance limits. The low energy scalar potential is given by $V = V_1 + V_2$, where for the doublets Ξ_1 and Ξ_2 we'll take the simple CP-conserving potential given by:

$$\begin{aligned} V_1 = {} & m_{11}^2 \Xi_1^\dagger \Xi_1 + m_{22}^2 \Xi_2^\dagger \Xi_2 - m_{12}^2 \left(\Xi_1^\dagger \Xi_2 + \Xi_2^\dagger \Xi_1 \right) \\ & + \frac{\lambda_1}{2} \left(\Xi_1^\dagger \Xi_1 \right)^2 + \frac{\lambda_2}{2} \left(\Xi_2^\dagger \Xi_2 \right)^2 + \lambda_3 \Xi_1^\dagger \Xi_1 \Xi_2^\dagger \Xi_2 \\ & + \lambda_4 \Xi_1^\dagger \Xi_2 \Xi_2^\dagger \Xi_1 + \frac{\lambda_5}{2} \left[\left(\Xi_1^\dagger \Xi_2 \right)^2 + \left(\Xi_2^\dagger \Xi_1 \right)^2 \right], \end{aligned} \quad (1)$$

with all parameters real while for the second part involving the singlet φ we will take simply:

$$\begin{aligned} V_2 = {} & \mu_\varphi^2 \varphi^2 + \frac{\lambda_\varphi}{2} \varphi^4 \\ & + \lambda_7 \varphi^2 \Xi_1^\dagger \Xi_1 + \lambda_9 \varphi^2 \Xi_2^\dagger \Xi_2. \end{aligned} \quad (2)$$

Note that after Electroweak Symmetry Breaking (EWSB), the above scalar potential induces a mixing between the neutral scalar components of Ξ_1 and Ξ_2 and the singlet φ. As a result, the field content of the model arises from the three field mass eigenstates from this mixing: h, H and H_3, together with the pseudo scalar A and the electrically charged scalar H^+.

From the minimization conditions we eliminate m_{11}^2, m_{22}^2 and μ_φ^2 in terms of the remaining parameters, this however only means we would be sitting in an extreme of the potential. To ensure that the values of the parameters correspond in fact to a minimum, we check numerically during the scan of parameter space the stability of the potential at a given point using the public tool EVADE [2, 3], which features the minimization of the scalar potential through polynomial homotopy continuation [4] and an estimation of the decay rate of a false vacuum [5,6]. We apply a hard cut on the parameter points that do not satisfy the stability criteria.

From the scalar potential, we obtain the mass matrices for the different scalar particles. The charged and pseudoscalar cases contain the two SM massless Goldstone states (the longitudinal modes of the SM massive gauge bosons). The physical particles have masses given by:

$$M_A^2 = m_{12}^2 \csc\beta \sec\beta - v^2 \lambda_5, \quad (3)$$

$$M_{H^\pm}^2 = m_{12}^2 \csc\beta \sec\beta - \frac{1}{2} v^2 (\lambda_4 + \lambda_5), \quad (4)$$

where $\tan\beta = v_{\Xi_2}/v_{\Xi_1}$ is the quotient of the vevs of the doublets, v_φ and v are the φ and the SM vevs respectively. For the CP-even neutral scalars, we can write the mass matrix as:

$$M_{\text{scalar}}^2 = \begin{pmatrix} a & d & f \\ d & b & e \\ f & e & c \end{pmatrix}, \quad (5)$$

with

$$\begin{aligned} a &= m_{12}^2 \tan\beta + \lambda_1 v^2 \cos^2\beta, \\ b &= m_{12}^2 \cot\beta + \lambda_2 v^2 \sin^2\beta, \\ c &= \lambda_\phi v_\phi^2, \\ d &= -m_{12}^2 + \lambda_{345} v^2 \cos\beta \sin\beta, \\ e &= \lambda_9 v v_\phi \sin\beta, \\ f &= \lambda_7 v v_\phi \cos\beta. \end{aligned} \quad (6)$$

The neutral scalar mass matrix is diagonalized by the mixing matrix Z^H such that

$$\text{diag}(m_h^2, m_H^2, m_{H3}^2) = Z^H M_{\text{scalar}}^2 Z^{H\text{T}}. \quad (7)$$

We find for the masses [7]:

$$\begin{aligned} m_h^2 &= \frac{1}{3} \left(a + b + c - 2\sqrt{x_1} \cos\left[\Xi_s/3 \right] \right), \\ m_H^2 &= \frac{1}{3} \left(a + b + c + 2\sqrt{x_1} \cos\left[(\Xi_s - \pi)/3 \right] \right), \\ m_{H_3}^2 &= \frac{1}{3} \left(a + b + c + 2\sqrt{x_1} \cos\left[(\Xi_s + \pi)/3 \right] \right), \end{aligned} \quad (8)$$

where

$$x_1 = a^2 + b^2 + c^2 - ab - ac - bc + 3(d^2 + f^2 + e^2), \quad (9)$$

and

$$\Xi_s = \begin{cases} \arctan\left(\frac{\sqrt{4x_1^3 - x_2^2}}{x_2} \right) & x_2 > 0, \\ \pi/2 & x_2 = 0, \\ \arctan\left(\frac{\sqrt{4x_1^3 - x_2^2}}{x_2} \right) + \pi & x_2 < 0, \end{cases} \quad (10)$$

with

$$\begin{aligned} x_2 = {} & -(2a - b - c)(2b - a - c)(2c - a - b) \\ & - 54def + 9[(2c - a - b)d^2 + (2b - a - c)f^2 \\ & + (2a - b - c)e^2]. \end{aligned} \quad (11)$$

Note that $\Xi_s \in [-\pi/2, 3\pi/2]$ so m_H^2 is always grater than m_h^2 but m_{H3}^2 can be smaller than m_h, this is an attractive feature of the model since there are some potential excesses in searches for light Higgs bosons reported by CMS [8]. We take into account experimental constraints from scalar searches at colliders using the public tool HiggsBounds

[9, 10] and applying a hard cut on parameter space points not complying with these limits. For the numerical computations we implement the model in SARAH [11-14] from which we generate corresponding model files for some of the other tools using the SARAH-SPheno framework [15-17]. When testing a given point of parameter space, for positivity and stability of the scalar potential we use EVADE, while exclusion limits from scalar searches at Tevatron, LEP and the LHC are implemented with the aid of HiggsBounds [10]. We impose hard cuts discarding points not complying with these constraints. For points not filtered by the previous hard cuts, we calculate numerically the model predicted observables that are used to construct a composite likelihood function. We calculate the couplings and decay branching ratios of the 125 GeV SM Higgs-like and the rest of the scalars with the help of the SARAH generated SPheno code. For the numerical calculation of the relic density, we use the capabilities of Micromegas [18-21]. Finally, we perform the scan of the parameter space and construct the likelihood profiles using Diver [22, 23] (in standalone mode).

We include the information from the measured values of the relic density $\Omega h^2_{\text{Planck}}$ and Higgs mass m_h as basic Gaussian likelihoods $\mathcal{L}_\Omega$ and $\mathcal{L}_{m_h}$ respectively. We also include a likelihood function $\mathcal{L}_{DD}$ based on results from the XENON1T Direct Detection Experiment, we then maximize over the model's parameter space the composite log-likelihood

$$\log \mathcal{L} = \log \mathcal{L}_{\text{DD}} + \log \mathcal{L}_\Omega + \log \mathcal{L}_{m_h}. \tag{12}$$

In Fig. 1 we present the low energy scalar mass spectra of the model, the regions of parameter space that better match high values of the composite log-likelihood are shown as bright zones, and the best fit point (BFP) is marked with a star. For the best fit point, we find that x_2 Eq. (11) is negative and in turn Ξ_s is very close to π. We thus find that the scalar H is markedly heavier than H_3, which is around twice as heavy as the SM-like Higgs h. Note that preferred values of the charged scalar $H^\pm$ mass are around 400 GeV, however there are zones that also have high values of the likelihood function below 200 GeV.

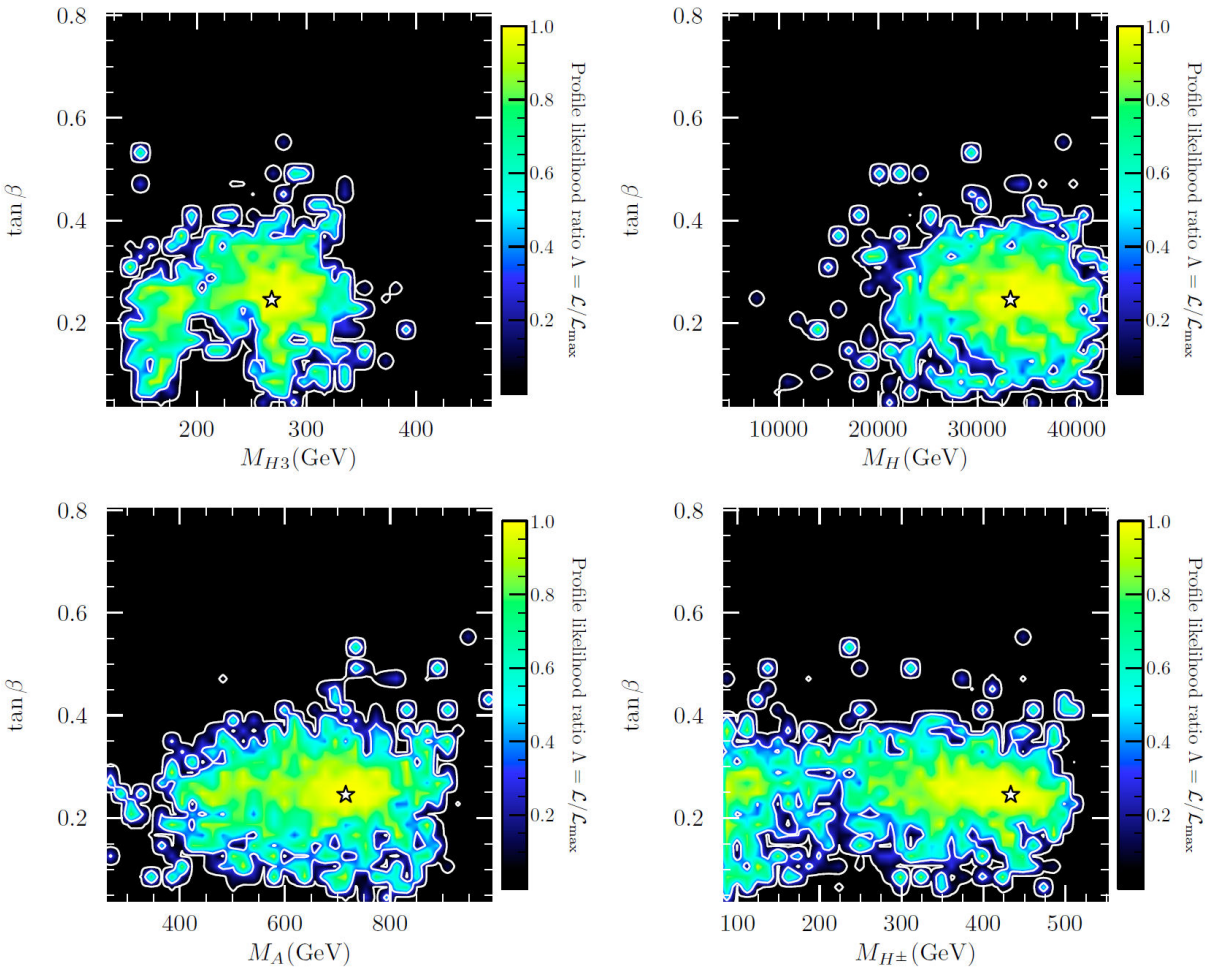

FIGURE 1. Composite likelihoods as functions of the scalar masses and $\tan\beta$. Contours of 68% and 95% of CL are drawn and the best fit point is marked with a star.

For this model, the DM candidate Ψ couples to fermions thanks to the mixing between the scalars through a coupling $y_\Omega \bar{\Psi}\Psi\varphi$. For simplicity, we will assume the DM Yukawa coupling y_Ω to be real. In the left panel of Fig. 2 we present the likelihood profile as a function of the mass of the DM candidate and its relic density (but not including the likelihood from the relic density, the corresponding plot with the full log-likelihood is just a slim horizontal bright band around the Planck measured value). We infer from this figure that DM candidate masses below ~ 2.5 TeV predict relic abundances greater than the observed Planck value of 0.12 which would imply an overproduction of DM during the freeze out epoch, and thus are excluded despite having a band of points compatible with other observables such as *e.g.* direct detection limits. We observed also that, assuming the DM candidate comprises 100% of the dark matter of the universe, its mass can only be around ~ 2.5 and ~ 20 TeV.

The DM candidate couples to fermions thanks to the mixing between the scalars. For simplicity, we will assume the DM Yukawa coupling y_Ω to be real, then the only parity conserving effective DM-quark interactions mediated by the physical scalars take the general form:

$$L_{\text{eff}} = \sum_k \overline{\Psi_R^C} c_\Psi^k \Psi_R \; h_k + \sum_{k,q} \overline{q} c_q^k q \; h_k, \tag{13}$$

where the sums are over the quark fields q and the physical scalars $h_k = h, H, H_3$. The effective couplings c_Ψ^k and c_q^k are functions of the free parameters and can be obtained explicitly from the Feynman rules of the model, we find ($k, q = 1, 2, 3$ and no summation over repeated indices):

$$c_\Psi^k = Z_{k3}^H \, y_\Omega, \tag{14}$$

and for d, s and b type quarks:

$$c_q^k = \frac{1}{2} Z_{k2}^H \left(\lambda^8 \, x_{11}^{(d)} \, U_{q1}^{dR} \, U_{q1}^{dL} + \lambda^3 \, x_{33}^{(d)} \, U_{q3}^{dR} \, U_{q3}^{dL} + U_{q2}^{dR} \left[\lambda^5 \, x_{22}^{(d)} \, U_{q2}^{dL} + \lambda^6 \, x_{12}^{(d)} \, U_{q1}^{dL} \right] \right) + \text{c.c.}, \tag{15}$$

while for u, c and t quarks we have:

$$c_q^k = \frac{1}{2} \left(\lambda^8 \, x_{11}^{(u)} \, U_{q1}^{uR*} \, U_{q1}^{uL*} \, Z_{k1}^H + \lambda^4 \, x_{22}^{(u)} \, U_{q2}^{uR*} \, U_{q2}^{uL*} \, Z_{k1}^H + U_{q3}^{uR*} \left[\left\{ \lambda^2 \, x_{23}^{(u)} \, U_{q2}^{uL*} + \lambda^4 \, x_{13}^{(u)*} \, U_{q1}^{uL*} \right\} Z_{k2}^H + x_{33}^{(u)} \, U_{q3}^{uL*} \, Z_{k1}^H \right] \right) + \text{c.c.}, \tag{16}$$

where we have denoted the quark mixing matrices by $U^{f(L,R)}$ to avoid index cluttering and λ is the Wolfenstein parameter. The quark Yukawa couplings $x^{(u/d)}$ are listed in Ref. [1], from which we obtain the DM-nucleon differential scattering cross section (in the non-relativistic limit):

$$\frac{d\sigma_N}{dE_R} = \frac{1}{32\pi M_\Psi m_N v^2} \; \left| \overline{\mathcal{M}} \right|^2, \tag{17}$$

here E_R is the nucleon recoil energy, m_N the nucleon mass and v the DM velocity. The scattering amplitud $\overline{\mathcal{M}}$ (averaged over initial spins and summed over final spins) receives the contribution of three diagrams (one for each scalar mediator) of the form:

$$\mathcal{M}_k = \frac{4 M_\Psi m_N}{q^2 + m_{h_k}^2} c_\Psi^k c_N^k \; \delta_{ss'} \delta_{rr'}, \tag{18}$$

where s, s' and r, r' denote DM and nucleon spin indices respectively, q is the momentum transfer, m_{h_k} the mass of the scalar mediators and c_N^k is defined as

$$c_N^k = \sum_q \frac{m_N}{m_q} c_q^k f_{T_q}^N, \tag{19}$$

with m_q the quark valence masses and $f_{T_q}^N$ expresses the quark-mass contributions to the nucleon mass. Numerical values for the latter can be found, *e.g.*, in Ref. [24] and references therein. The momentum transfer is related to the recoil energy through $q^2 = 2 m_N E_R$, so that the total DM-nucleon spin independent cross section reads:

$$\sigma_N^{\text{SI}} = \int_0^{E_R^{\max}} \frac{d\sigma_N}{dE_R} dE_R, \tag{20}$$

with the maximum recoil energy given by

$$E_R^{\max} = \frac{2 v^2 \mu^2}{m_N}, \tag{21}$$

μ being the DM-nucleon reduced mass.

We now present a likelihood analysis involving publicly available data from the direct dectection XENON1T experiment [25]. We make use of the capabilities of the numerical tool `DDCalc` to compute the Poisson likelihood given by

$$\mathcal{L}_{\text{DD}} = \frac{(b+s)^o e^{-(b+s)}}{o!}, \tag{22}$$

where o is the number of observed events in the detector and b is the expected background count. From the model's predicted DM-nucleon cross sections Eq. (20) as input, `DDCalc` computes the number of expected signal events s for given DM local halo and velocity distribution models (we use the tool's default models, for specific details on the implementation such as simulation of the detector efficiencies and acceptance rates, possible binning etc. see [27, 28]). In the right panel of Fig. 2, we present the profile likelihood normalized to the value of $\mathcal{L}$ at the best fit point (signaled by a star) assuming the DM candidate constitutes 100% of the DM in the Universe. The plot shows the dependence of the likelihood on the DM mass and the DM-proton spin independent (SI) cross section; contours of 68% and 95% of confidence level (CL) are drawn. We also depict the 90% CL upper limit on the SI cross section from the XENON1T (1t $\times$ yr) experiment [25], alongside with the multi ton-scale time projection to 200 t $\times$ yr of reference [29] and an estimation of the neutrino floor [30]. We note that almost all the region consistent

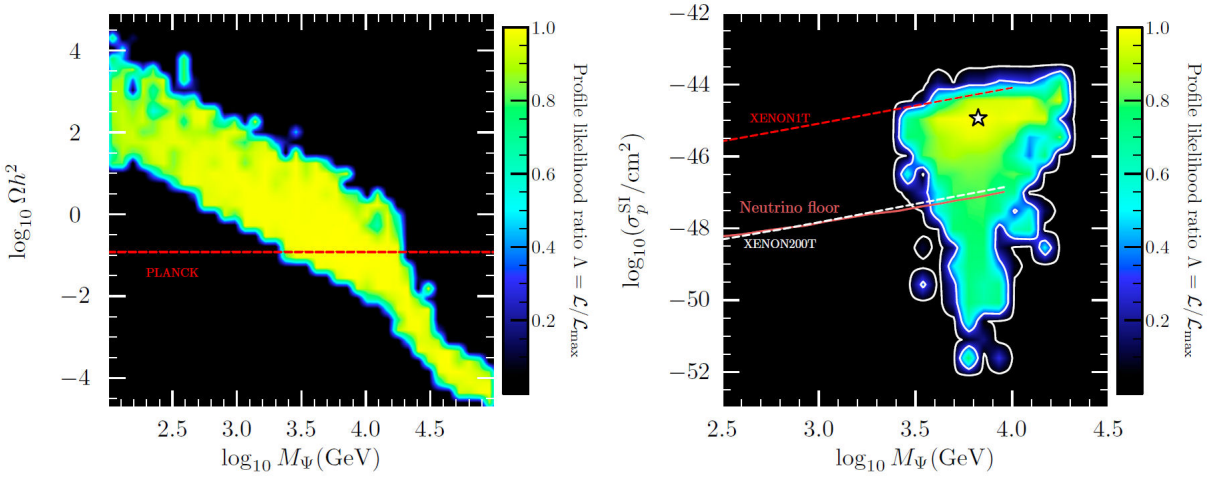

FIGURE 2. Left panel: Composite likelihood (not including the relic density likelihood) as a function of the DM candidate mass and its relic density. The Planck measured value [26] is marked by the dashed horizontal line. Right panel: Composite likelihood as a function of the DM candidate mass and SI DM-proton cross section for the case that the candidate represents 100% of the DM in the Universe. Contours of 68% and 95% of CL are drawn, and also shown are the 90% CL upper limit from the 1t×1yr XENON1T experiment, the multi ton projection to 200t×1yr and the neutrino floor. The best fit point is marked with a star.

with the constraints including the BFP (at a mass of ~ 6.66TeV corresponding to a cross section of $\sim 1.14 \times 10^{-45}$ cm^2) lies below the zone currently excluded by the XENON1T experiment. However, the figure also makes it evident that the multi ton projection to 200t×1yr will be capable of probing zones well below the BFP of the model.

3. Conclusions

We have presented analysis of the scalar and DM sectors of a BSM model featuring a discrete $Q4$ symmetry and a fermion DM candidate. The consistency of our model with the constraints arising from collider searches for heavy scalars, stability of the scalar potentials, the dark matter relic density and current and future direct detection experiments sets stringent limits on the parameter space of the model. In particular, in this kind of models where the discrete symmetry is also present in the scalar sector, the analysis of the characteristics and phenomenology gives rise to constraints that enlarge the set of usual ones from the matter sector such as, *e.g.*, FCNC.

Acknowledgements

C.E. acknowledges the support of Conahcyt (México) Cátedra no. 341. This research is partially supported by DGAPA PAPIIT IN109321.

1. A. E. Cárcamo Hernández *et al.*, Fermion masses and mixings, dark matter, leptogenesis and g - 2 muon anomaly in an extended 2HDM with inverse seesaw, *Eur. Phys. J. Plus* **137** (2022) 1224, https://doi.org/10.1140/epjp/s13360-022-03432-w.

2. P. M. Ferreira *et al.*, Vacuum Instabilities in the N2HDM, *JHEP* **2019** (2019) 6, https://doi.org/10.1007/JHEP09(2019)006.

3. W. G. Hollik, G.Weiglein, and J. Wittbrodt, Impact of Vacuum Stability Constraints on the Phenomenology of Supersymmetric Models, *JHEP* **2019** (2019) 109, https://doi.org/10.1007/JHEP03(2019)109.

4. M. Maniatis and D. Mehta, Minimizing Higgs Potentials via Numerical Polynomial Homotopy Continuation, *Eur. Phys. J. Plus* **127** (2012) 91, https://doi.org/10.1140/epjp/i2012-12091-1.

5. S. Coleman, The Fate of the False Vacuum: Semiclassical Theory, *Phys. Rev. D* **15** (1977) 2929, https://doi.org/10.1103/PhysRevD.15.2929.

6. C. G. Callan, Jr. and S. R. Coleman, The Fate of the False Vacuum. II. First Quantum Corrections, *Phys. Rev. D* **16** (1977) 1762, https://doi.org/10.1103/PhysRevD.16.1762.

7. C.-A. Deledalle *et al.*, Closed-form expressions of the eigen decomposition of 2 x 2 and 3 x 3 Hermitian matrices, Research report, Université de Lyon (2017), https://hal.archives-ouvertes.fr/hal-01501221.

8. A. M. Sirunyan *et al.*, Search for a standard model-like Higgs boson in the mass range between 70 and 110 GeV in the diphoton final state in proton-proton collisions at $\sqrt{s}$ = 8 and 13 TeV, *Phys. Lett. B* **793** (2019) 320, https://doi.org/10.1016/j.physletb.2019.03.064.

9. P. Bechtle *et al.*, Applying Exclusion Likelihoods from LHC Searches to Extended Higgs Sectors, *Eur. Phys. J.*

C **75** (2015) 421, https://doi.org/10.1140/epjc/s10052-015-3650-z.

10. P. Bechtle *et al*., HiggsBounds-5: Testing Higgs Sectors in the LHC 13 TeV Era, *Eur. Phys. J. C* **80** (2020) 1211, https://doi.org/10.1140/epjc/s10052-020-08557-9.
11. F. Staub, Automatic calculation of supersymmetric renormalization group equations and loop corrections, *Comput. Phys. Commun.* **182** (2011) 808, https://doi.org/10.1016/j.cpc.2010.11.030.
12. F. Staub, From Superpotential to Model Files for FeynArts and CalcHep/CompHep, *Comput. Phys. Commun.* **181** (2010) 1077, https://doi.org/10.1016/j.cpc.2010.01.011.
13. F. Staub, Automatic Calculation of supersymmetric Renormalization Group Equations and Self Energies, *Comput. Phys. Commun.* **182** (2011) 808, https://doi.org/10.1016/j.cpc.2010.11.030.
14. F. Staub, SARAH 3.2: Dirac Gauginos, UFO output, and more, *Comput. Phys. Commun.* **184** (2013) 1792, https://doi.org/10.1016/j.cpc.2013.02.019.
15. F. Staub, Exploring new models in all detail with SARAH, *Adv. High Energy Phys.* **2015** (2015) 840780, https://doi.org/10.1155/2015/840780.
16. W. Porod, SPheno, a program for calculating supersymmetric spectra, SUSY particle decays and SUSY particle production at e+ e- colliders, *Comput. Phys. Commun.* **153** (2003) 275, https://doi.org/10.1016/S0010-4655(03)00222-4.
17. W. Porod and F. Staub, SPheno 3.1: Extensions including flavour, CP-phases and models beyond the MSSM, *Comput. Phys. Commun.* **183** (2012) 2458, https://doi.org/10.1016/j.cpc.2012.05.021.
18. G. Bélanger *et al.*, micrOMEGAs_3: A program for calculating dark matter observables, *Comput. Phys. Commun.* **185** (2014) 960, https://doi.org/10.1016/j.cpc.2013.10.016.
19. G. Bélanger *et al*., micrOMEGAs4.1: two dark matter candidates, *Comput. Phys. Commun.* **192** (2015) 322, https://doi.org/10.1016/j.cpc.2015.03.003.
20. D. Barducci *et al*., Collider limits on new physics within micrOMEGAs_4.3, *Comput. Phys. Commun*. **222** (2018) 327, https://doi.org/10.1016/j.cpc.2017.08.028.
21. G. Bélanger *et al*., micrOMEGAs5.0 : Freeze-in, *Comput. Phys. Commun.* **231** (2018) 173, https://doi.org/10.1016/j.cpc.2018.04.027.
22. G. D. Martinez *et al.*, Comparison of statistical sampling methods with ScannerBit, the GAMBIT scanning module, *Eur. Phys. J. C* **77** (2017) 761, https://doi.org/10.1140/epjc/s10052-017-5274-y.
23. P. Scott, Pippi - painless parsing, post-processing and plotting of posterior and likelihood samples, *Eur. Phys. J. Plus* **127** (2012) 138, https://doi.org/10.1140/epjp/i2012-12138-3.
24. E. Del Nobile, The Theory of Direct Dark Matter Detection: A Guide to Computations (2021), https://doi.org/10.1007/978-3-030-95228-0.
25. E. Aprile *et al.*, Dark Matter Search Results from a One Ton-Year Exposure of XENON1T, *Phys. Rev. Lett.* **121** (2018) 111302, https://doi.org/10.1103/PhysRevLett.121.111302.
26. N. Aghanim *et al*., Planck 2018 results. VI. Cosmological parameters, *Astron. Astrophys.* **641** (2020) A6, https://doi.org/10.1051/0004-6361/201833910.
27. T. Bringmann *et al*., DarkBit: A GAMBIT module for computing dark matter observables and likelihoods, *Eur. Phys. J. C* **77** (2017) 831, https://doi.org/10.1140/epjc/s10052-017-5155-4.
28. P. Athron *et al*., Global analyses of Higgs portal singlet dark matter models using GAMBIT, *Eur. Phys. J. C* **79** (2019) 38, https://doi.org/10.1140/epjc/s10052-018-6513-6.
29. M. Schumann *et al*., Dark matter sensitivity of multi-ton liquid xenon detectors, *JCAP* **10** (2015) 016, https://doi.org/10.1088/1475-7516/2015/10/016.
30. J. Billard, L. Strigari, and E. Figueroa-Feliciano, Implication of neutrino backgrounds on the reach of next generation dark matter direct detection experiments, *Phys. Rev. D* **89** (2014) 023524, https://doi.org/10.1103/PhysRevD.89.023524.